Antimicrobial properties of novel ionic liquids derived from imidazolium cation with phenolic functional groups

Luis Guzmán [a], Cristóbal Parra-Cid [a], Etiennette Guerrero-Muñoz [b], Carlos Peña-Varas [c], Efraín Polo-Cuadrado [d], Yorley Duarte [e], Ricardo I. Castro [f], Luz Stella Nerio [g], Ramiro Araya-Maturana [b], Tewodros Assefa [h,i], Javier Echeverría [j], David Ramírez [c], Oscar Forero-Doria [j,*]

[a] Departamento de Bioquímica Clínica e Inmunohematología, Facultad de Ciencias de la Salud, Universidad de Talca, P.O. Box 747, Talca 3460000, Chile
[b] Instituto de Química de Recursos Naturales, Universidad de Talca, P.O. Box 747, Talca 3460000, Chile
[c] Instituto de Ciencias Biomédicas, Facultad de Ciencias de la Salud, Universidad Autónoma de Chile, El Llano Subercaseaux, 2801-Piso 6, Santiago, Chile
[d] Instituto de Química de Recursos Naturales, Laboratorio de Síntesis Orgánica, Universidad de Talca, Casilla 747, Talca 3460000, Chile
[e] Center for Bioinformatics and Integrative Biology, Facultad de Ciencias de la Vida, Universidad Andres Bello, Santiago, Chile
[f] Carrera de Ingeniería en Construcción e Instituto de Ciencias Químicas Aplicadas, Multidisciplinary Agroindustry Research Laboratory, Universidad Autónoma de Chile, Talca, Chile
[g] Universidad de la Amazonia, Programa de Química, Calle 17 Diagonal 17 Carrera 3F, Florencia, Colombia
[h] Department of Chemistry and Chemical Biology, Rutgers, The State University of New Jersey, 610 Taylor Road, Piscataway, NJ 08854, United States
[i] Department of Chemical and Biochemical Engineering, Rutgers, The State University of New Jersey, 98 Brett Road, Piscataway, NJ 08854, United States
[j] Departamento de Ciencias del Ambiente, Facultad de Química y Biología, Universidad Santiago de Chile, Santiago, Chile

ARTICLE INFO

ABSTRACT

Bacterial infections are nowadays among the major threats to public health worldwide. Thus, there is an urgent and increased need for new antimicrobial agents. As a result, the exploration of the antimicrobial properties of different substances including ionic liquids (ILs) has recently attracted great attention. The present work is aimed at evaluating how the addition of halogens and hydrophobic substituents on alkylimidazolium units of ILs as well as the increase in their chain lengths affects the antimicrobial properties of such ILs. After their synthesis, the antibacterial activities of these compounds against *Pseudomona aeruginosa*, *Escherichia coli*, and *Staphylococcus aureus* are determined by measuring their minimal inhibitory concentrations (MICs). Key features in ILs-membrane interactions are also studied using long-term all-atom molecular dynamics simulations (MDs). The results show that these ILs have good antibacterial activity against *S. aureus*, *E. coli*, and *P. aeruginosa*, with MIC values range from <7.81 to 62.50 μM. The antimicrobial property of *tert*-butyl *N*-methylphenolimidazolium salts (denoted as **8b** and **8c**) is particularly better with MIC values of < 7.81 μM. The antibacterial efficacy is also found to depend on the alkyl chain length and substituents on the phenolic ring. Finally, MDs done for ILs in a phosphatidylcholine (POPC) bilayer show key features in the mechanism of IL-induced membrane disruption, where the ILs are inserted as clusters into one side of the bilayer until saturation is reached. This insertion increases "leaflet strain" up to critical threshold, likely triggering the morphological disruption of the membranes in the microbes.

1. Introduction

Nowadays, some of the major threats to public health are associated with nosocomial infections, which account for almost 37,000 deaths in the USA and are continuously increasing worldwide [1]. Frequently, nosocomial infections are caused by the normal microbiota of the patient moving to the site of infection during/due to surgical or medical procedures. Nosocomial infections are most commonly caused by bacteria including *S. aureus* (which is one of the main bacteria causing infections at surgical sites), *E. coli* (which is the main agent responsible for many catheter-associated urinary tract infections), and *P. aeruginosa* (which is associated with respiratory and bloodstream infections,

especially in premature neonates and burn and intubated patients) [2]. Therefore, there is an urgent need to develop new, potent antimicrobial agents that can inhibit or prevent the growth of such bacteria, which are prevalent and cause nosocomial infections.

The antimicrobial properties of ionic liquids (ILs) have attracted the attention of researchers and become a subject of major studies in recent years. ILs are salts that have a melting point of up to 100 °C [3]. Many of them are liquids at room temperature due to their bulky, asymmetric cations, and weakly coordinating anions that destabilize their crystal lattice. Their physicochemical properties render them vanishingly low vapor pressure and several layers of solvation, and thereby a unique ability to interact with different types of molecules [4]. ILs with rationally designed biological properties can be synthesized from cationic derivatives of neutral imidazole heterocycles and organic anions via various synthetic routes [5].

The biological activity of a given IL may vary from one organism to another. It can also depend on its solubility in solutions and its interaction with the solvent. The solubility of an IL varies depending on the size of its cation, anion and sometimes, the aromaticity of its rings. For example, in water, imidazolium ILs are highly soluble, pyrrolidinium and pyridinium ILs are only moderately soluble, and piperidinium ILs are poorly soluble;[6] meanwhile, counter anions as chloride ([Cl]⁻), bromide ([Br]⁻), and tetrafluoroborate ([BF$_4$]⁻) anions strongly interact with water molecules, hexafluorophosphate ([PF$_6$]⁻) anion does not do so [7]. Therefore, the ions involved in the ILs affect not only the solubility but also the biological properties, toxicity, and biodegradation of ILs [8]. They can also dictate their interactions with biological membranes and the potential applications of ILs in biological systems. A recent investigation showed that imidazolium and benzimidazolium salts could function as transmembrane anion transporters, cause an electrolytic imbalance, disrupt the integrity and the membrane potential in the bacteria, and exhibit low cytotoxicity in the range of bacteriostatic concentrations [9]. Another study, which used coarse-grained molecular dynamics simulations (CG-MDs), revealed the key features associated with the mechanism of IL-induced membrane disruption [10]. Notably, the study indicated that ILs could insert themselves into one side of the bilayer membrane reaching a saturation limit. This, in turn, increased "leaflet strain" until the critical threshold, thus initiating a morphological alteration of the membrane [10].

Several chemical synthetic strategies have been used to produce ILs. The most commonly used methods include metathesis of a halide salt with a metal or an ammonium salt, acid-base neutralization reaction, or direct combination reaction [11]. Although these traditional reactions can efficiently produce ILs, they involve highly polluting chemicals as solvents, which can negatively impact the environment. Therefore, new greener methods that result in no/less chemical contaminants and cause no/minimal environmental impact are currently of great interest [12,13].

Microwave (MW) synthesis has recently been introduced as an efficient approach, to produce ILs, in high yields and in shorter reaction times [14]. A series of alkylimidazolium ILs that are synthesized in three step of reaction, have also been tested as antibacterial agents against pathogens that cause skin and soft tissue infections (SSTI), and their performances have been satisfactory [14]. The present work is aimed at evaluating the effects of halogens, hydrophobic substituents and alkyl chain lengths present on alkylimidazolium units of ILs on the antimicrobial properties of the ILs. To achieve the objective, a series of ILs with different such groups are synthesized and their antibacterial activities against *Pseudomona aeruginosa*, *Escherichia coli*, and *Staphylococcus aureus* are then determined. Moreover, key features in the ILs-membrane interactions are studied using MDs over long timescales and the results are included.

2. Experimental section

2.1. General Information.

Reagents needed for the synthesis of ILs were obtained from Sigma-Aldrich (St. Louis, MO, USA). ^{1}H and ^{13}C NMR spectra (400 MHz for proton and 100 MHz for carbon) were recorded using an AM-400 NMR spectrometer (Bruker, Rheinstetten, Germany). High-resolution mass spectrometry (ESI-MS and ESI-MS/MS) were performed using a high-resolution hybrid quadrupole (Q) and orthogonal time-of-flight (TOF) mass spectrometer (Waters/Micromass Q-TOF micro, Manchester, UK). The experiments were conducted at a constant nebulizer temperature of 100 °C.

2.2. Chemical Synthesis.

General Procedure Applied for the Synthesis of Different N-Methyl-phenolimidazoles, 5a-c. In a typical synthesis of different *N-Methyl-phenolimidazoles*, typically, 5 mmol of imidazole, 5 mmol of paraformaldehyde and 3.0 mL of tetrahydrofuran (THF) were mixed together in a reaction flask (see Scheme 1). THF was used as a solvent. The mixture was stirred with a magnetic bar. While being stirred, the mixture was heated in the microwave reactor at 200 W at 120 °C for 5 min. The resulting clear solution containing hemiaminal was concentrated at room temperature. Prior to purification, it was charged with 5 mmol of phenol (namely, 4-fluorphenol (**4a**), 4-chlorophenol (**4b**) or 2-terbutyl-4-methoxyphenol (**4c**)), dissolved in dioxane/H$_2$O solution (1:1), and microwaved at 200 W at 120 °C for 5 min (see Scheme 1). The resulting oily residue was subject to column chromatography using hexane/EtOAc (7:3). The yields of the products **5a**, **5b** and **5c** were 60, 65 and 90%, respectively.
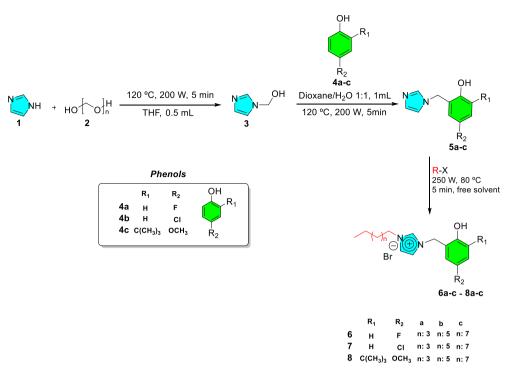
General Procedure Applied for the Synthesis of Different N-Methyl-phenolimidazolium Salts. Next, a quaternization reaction was carried out by mixing the different *N-Methylphenolimidazoles* synthesized above, **5a-c** (1 mmol), and three different alkyl bromides (hexyl, octyl, and decyl) (1.5 mmol) and then treating the mixture under microwave radiation (250 MW) at 80 °C for 10 min under solvent-free condition (Scheme 1). The reaction completion was marked by the separation of dense ILs. The ILs composed of *N*-methylimidazolium salts **6a-c** – **8a-c** (Scheme 1) were isolated using toluene as a solvent and decanting the supernatant, along with any unreacted starting materials. Subsequently, the ILs were rinsed with diethyl ether (4 × 10 mL) and the bottom layer was kept after decantation. In each case, the ILs were finally dried under reduced (4 h) pressure to get rid of any volatile organic compounds in them.

2-((1*H*-imidazol-1-yl)methyl)-4-fluorophenol (**5a**). 60% yield. ^{1}H NMR (400 MHz, CD$_3$OD): 4.86 (s, 2H), 6.71–6.75 (m, 3H), 6.83–6.88 (m, 3H); HRMS (ESI, *m/z*): Calcd. for C$_{10}$H$_9$FN$_2$O$^+$ 192.0699 [M]$^+$; Found 192.0700

2-((1H-imidazol-1-yl)methyl)-4-chlorophenol (**5b**) [15]. 65% yield. ^{1}H NMR (400 MHz, CD$_3$OD): 4.86 (s, 2H), 6.71–6.75 (m, 3H), 7.09–7.12 (m, 3H); HRMS (ESI, *m/z*): Calcd. for C$_{10}$H$_9$ClN$_2$O$^+$ 208.0403 [M]$^+$; Found 208.0421

2-((1*H*-imidazol-1-yl)methyl)-6-(*tert*-butyl)-4-methoxyphenol (**5c**). 90% yield. ^{1}H NMR (400 MHz, CD$_3$OD): 1.39 (s, 9H), 3.69 (s, 3H), 4.85 (s, 2H), 6.56–6.59 (m, 1H), 6.65–6.67 (m, 1H), 6.79–6.80 (m, 1H); ^{13}C NMR (100 MHz, CD$_3$OD): 29.9 (3 × CH$_3$), 35.5 (C), 56.1 (CH$_3$), 111.6 (CH), 114.5 (CH), 117.3 (CH), 138.2 (CH), 151.0 (C), 153.8 (C); HRMS (ESI, *m/z*): Calcd. for C$_{15}$H$_{20}$N$_2$O$_2$$^+$ 260.1525 [M]$^+$; Found 260.1511

1-(5-Fluoro-2-hydroxybenzyl)-3-hexyl-1*H*-imidazol-3-ium bromide (**6a**). 73% yield. ^{1}H NMR (400 MHz, CD$_3$OD); 0.88–0.91 (m, 3H), 1.34 (bs, 6H), 1.89–1.91 (m, 2H), 4.22–4.30 (m, 2H), 4.64 (s, 2H), 6.71–6.74 (m, 1H), 6.87 (t, *J* = 8.7 Hz, 1H), 7.58 (d, *J* = 7.6 Hz, 1H), 7.68–7.69 (m, 1H), 8.94–9.13 (m, 2H); ^{13}C NMR (100 MHz, CD$_3$OD): 14.3 (CH$_3$), 23.5 (CH$_2$), 26.9 (CH$_2$), 31.1 (CH$_2$), 32.2 (CH$_2$), 50.6 (CH$_2$), 50.9 (CH$_2$), 116.3, (CH, *J*$_{C-F}$ = 24.0 Hz), 116.6 (CH, *J*$_{C-F}$ = 8.0 Hz), 120.5 (CH), 121.1 (CH), 123.3 (CH), 123.8 (CH); HRMS (ESI, *m/z*): Calcd. for

Scheme 1. Synthesis of imidazolium ionic liquids (ILs) containing phenolic groups with different substituent chain lengths.

$C_{16}H_{23}FKN_2O^+$ 317,1426 [M−Br + K + H] $^+$; Found 317,2773.

1-(5-Fluoro-2-hydroxybenzyl)-3-octyl-1*H*-imidazol-3-ium bromide (**6b**). 68% yield. ^{1}H NMR (400 MHz, CD$_3$OD); 0.88 (t, *J* = 6.6 Hz, 3H), 1.28–1.34 (m, 10*H*), 1.88–1.93 (m, 2H), 4.25 (q, *J* = 7.3 Hz, 2H), 4.64 (s, 2H), 6.73 (dd, *J* = 4.3, 8.9 Hz, 1H), 6.87 (t, *J* = 8.7 Hz, 1H), 7.54–7.57 (m, 1H), 7.66–7.68 (m, 1H), 8.88–8.94 (m, 1H), 9.13 (s, 1H); ^{13}C NMR (100 MHz, CD$_3$OD); 14.4 (CH$_3$), 23.6 (CH$_2$), 27.2 (CH$_2$), 30.0 (CH$_2$), 30.2 (CH$_2$), 31.1 (CH$_2$), 32.8 (CH$_2$), 50.5 (CH$_2$), 50.9 (CH$_2$), 117.1 (CH, $J_{C\text{-}F}$ = 18 Hz), 123.2 (C, $J_{C\text{-}F}$ = 7.0 Hz), 123.8 (CH), 136.4 (CH), 137.1 (CH), 154.8 (2 × CH), 156.7 (C, $J_{C\text{-}F}$ = 18 Hz), 159.0 (C); HRMS (ESI, *m/z*): Calcd. for $C_{18}H_{25}FN_2Na_3O^+$ 373,1639 [M−Br−H + 3Na]$^+$; Found 373,3111.

3-Decyl-1-(5-fluoro-2-hydroxybenzyl)-1*H*-imidazol-3-ium bromide (**6c**). 65% yield. ^{1}H NMR (400 MHz, CD$_3$OD); 0.88 (t, *J* = 6.6 Hz, 3H), 1.28–1.34 (m, 14H), 1.88–1.91 (m, 2H), 4.22–4.29 (m, 2H), 4.67 (s, 2H), 6.72 (dd, *J* = 4.4, 8.8 Hz, 1H), 6.87 (t, *J* = 8.7 Hz, 1H), 7.57 (d, *J* = 8.1 Hz, 1H), 7.67 (s, 1H), 8.93–9.00 (m, 1H), 9.12 (s, 1H); ^{13}C NMR (100 MHz, CD$_3$OD); 14.4 (CH$_3$), 23.7 (CH$_2$), 27.2 (CH$_2$), 30.0 (CH$_2$), 30.4 (CH$_2$), 30.5 (CH$_2$), 30.6 (CH$_2$), 31.1 (CH$_2$), 33.0 (CH$_2$), 50.6 (CH$_2$), 50.9 (CH$_2$), 116.5 (CH, $J_{C\text{-}F}$ = 23.0 Hz), 117.1 (C, $J_{C\text{-}F}$ = 7.0 Hz), 120.5 (CH), 121.2 (CH), 123.3 (CH), 123.8 (CH), 137.1 (CH), 154.6 (C), 156.7 (C), 159.0 (C); HRMS (ESI, *m/z*): Calcd. for $C_{20}H_{29}BrFN_2Na_2O^+$ 457,1243 [M−H + 2Na]$^+$; Found 457,3025.

1-(5-Chloro-2-hydroxybenzyl)-3-hexyl-1*H*-imidazol-3-ium bromide (**7a**). 60% yield. ^{1}H NMR (400 MHz, CD$_3$OD); 0.88 (t, *J* = 6.2 Hz, 3H), 1.33 (bs, 6H), 1.89 (bs, 2H), 4.23–4.30 (m, 2H), 4.64 (s, 2H), 6.74 (d, *J* = 8.6 Hz, 1H), 7.11 (d, *J* = 8.8 Hz, 1H), 7.58–7.60 (m, 1H), 7.72–7.73 (m, 1H), 8.96–9.05 (m, 1H), 9.16 (s, 1H); ^{13}C NMR (100 MHz, CD$_3$OD); 16.9 (CH$_3$), 26.1 (CH$_2$), 29.4 (CH$_2$), 33.6 (CH$_2$), 34.8 (CH$_2$), 53.2 (CH$_2$), 53.5 (CH$_2$), 120.3 (CH), 123.1 (CH), 123.6 (CH), 125.9 (CH), 126.4 (CH), 127.5 (C), 132.8 (CH), 160.0 (C); HRMS (ESI, *m/z*): Calcd. for $C_{16}H_{22}ClN_2O^+$ [M−Br]$^+$ 293,1415; found 293,1424.

1-(5-Chloro-2-hydroxybenzyl)-3-octyl-1*H*-imidazol-3-ium bromide (**7b**). 67% yield. ^{1}H NMR (400 MHz, CD$_3$OD); 0.91 (t, *J* = 6.6 Hz, 3H), 1.29–1.34 (m, 10*H*), 1.88–1.93 (m, 2H), 4.22–4.29 (m, 2H), 6.73 (d, *J* = 8.8 Hz, 1H), 7.11 (d, *J* = 8.8 Hz, 1H), 7.57–7.60 (m, 1H), 7.67 (s, 1H), 8.93–9.01 (m, 1H), 9.11 (s, 1H); ^{13}C NMR (100 MHz, CD$_3$OD); 13.0 (CH$_3$), 22.2 (CH$_2$), 25.8 (CH$_2$), 28.6 (CH$_2$), 28.8 (CH$_2$), 29.7 (CH$_2$), 31.4

(CH$_2$), 49.1 (CH$_2$), 49.5 (CH$_2$), 116.3 (C), 119.1 (CH), 119.7 (CH), 121.9 (CH), 122.4 (CH), 128.8 (2 × CH); HRMS (ESI, *m/z*): Calcd. for $C_{18}H_{26}ClN_2O^+$ [M−Br]$^+$ 321,1728; found 321,1737.

1-(5-Chloro-2-hydroxybenzyl)-3-decyl-1*H*-imidazol-3-ium bromide (**7c**). 75% yield. ^{1}H NMR (400 MHz, CD$_3$OD); 0.88 (t, *J* = 6.6 Hz, 3H), 1.28–1.34 (m, 14H), 1.88–1.93 (m, 2H), 4.22–4.29 (m, 2H), 4.64 (s, 2H), 6.74 (d, *J* = 8.8 Hz, 1H), 7.11 (d, *J* = 8.6 Hz, 1H), 7.57–7.60 (d, *J* = 8.0 Hz, 1H), 7.68 (s, 1H), 8.94–9.02 (m, 1H), 9.13 (s, 1H); ^{13}C NMR (100 MHz, CD$_3$OD); 13.0 (CH$_3$), 22.3 (CH$_2$), 25.8 (CH$_2$), 28.6 (CH$_2$), 29.0 (CH$_2$), 29.2 (CH$_2$), 29.3 (CH$_2$), 29.7 (CH$_2$), 31.6 (CH$_2$), 49.2 (CH$_2$), 49.5 (CH$_2$), 116.3 (C), 119.1 (CH), 119.7 (CH), 121.9 (CH), 122.4 (CH), 128.8 (2 × CH); HRMS (ESI, *m/z*): Calcd. for $C_{20}H_{30}ClN_2O^+$ [M−Br]$^+$ 349,2041; found 349,2061.

1-(3-(*tert*-Butyl)-2-hydroxy-5-methoxybenzyl)-3-hexyl-1*H*-imidazol-3-ium bromide (**8a**). 75% yield. ^{1}H NMR (400 MHz, CD$_3$OD); 0.88–0.91 (m, 3H), 1.34–1.37 (m, 15H), 1.91–1.94 (m, 2H), 3.69 (s, 3H), 4.22–4.29 (m, 2H), 4.67 (s, 2H), 7.58 (d, *J* = 7.8 Hz, 1H), 7.67–7.69 (m, 1H), 8.94–9.02 (m, 2H), 9.12 (s, 1H); ^{13}C NMR (100 MHz, CD$_3$OD); 14.3 (CH$_3$), 23.4 (CH$_2$), 26.9 (CH$_2$), 29.9 (3x CH$_3$), 30.3 (CH$_2$), 31.0 (CH$_2$), 32.2 (C), 50.6 (CH$_2$), 50.9 (CH$_2$), 56.2 (CH$_3$), 111.8 (CH), 114.5 (CH), 117.4 (CH), 121.1 (CH), 123.3 (C), 123.8 (CH), 153.9 (C); HRMS (ESI, *m/z*): Calcd. for $C_{21}H_{33}N_2O_2^+$ [M−Br]$^+$ 345,2537; found 345,2548.

1-(3-(*tert*-Butyl)-2-hydroxy-5-methoxybenzyl)-3-octyl-1*H*-imidazol-3-ium bromide (**8b**). 82% yield. ^{1}H NMR (400 MHz, CD$_3$OD); 0.89 (t, *J* = 6.5 Hz, 3H), 1.29–1.38 (m, 21H), 1.88–1.91 (m, 2H), 3.69 (s, 3H), 4.22–4.27 (m, 2H), 4.64 (s, 2H), 7.55 (s, 1H), 7.67 (s, 1H), 8.85–8.89 (m, 2H), 9.11 (s, 1H); ^{13}C NMR (100 MHz, CD$_3$OD); 14.4 (CH$_3$), 23.6 (CH$_2$), 27.2 (CH$_2$), 29.9 (CH$_2$), 30.0 (CH$_2$), 30.2 (CH$_2$), 31.1 (2 × CH$_3$), 31.2 (CH$_3$), 32.8 (CH$_2$), 35.6 (C), 50.4 (CH$_2$), 50.9 (CH$_2$), 56.2 (CH$_3$), 117.4 (CH), 120.6 (CH), 121.7 (CH), 123.1 (CH), 123.8 (CH), 137.1 (C), 151.2 (C), 153.9 (C); HRMS (ESI, *m/z*): Calcd. for $C_{23}H_{37}N_2O_2^+$ [M−Br]$^+$ 373,2850; found 373,2838.

1-(3-(*tert*-Butyl)-2-hydroxy-5-methoxybenzyl)-3-decyl-1*H*-imidazol-3-ium bromide (**8c**). 87% yield. ^{1}H NMR (400 MHz, CD$_3$Cl); 0.87–0.90 (m, 3H), 1.28–1.38 (m, 25H), 1.88–1.91 (m, 2H), 3.69 (s, 3H), 4.22–4.29 (m, 2H), 4.64 (s, 2H), 7.59 (s, 1H), 7.67 (s, 1H), 8.93–9.01 (m, 2H), 9.12 (s, 1H); ^{13}C NMR (100 MHz, CD$_3$Cl); 14.4 (CH$_3$), 23.7 (CH$_2$), 27.2 (CH$_2$), 29.1 (CH$_2$), 30.5 (CH$_2$), 30.4 (CH$_2$), 30.6 (CH$_2$), 31.1 (CH$_2$), 33.0 (CH$_2$),

50.63 (CH$_2$), 50.9 (C), 56.2 (CH$_3$), 114.5 (CH), 117.4 (CH), 120.5 (CH), 121.1 (CH), 123.3 (C), 123.8 (CH), 137.1 (CH), 151.2 (C) 153.4 (C); HRMS (ESI, *m/z*): Calcd. for C$_{25}$H$_{41}$N$_2$O$_2$$^+$ [M−Br]$^+$ 401,3163; found 401,3179.

Thermal Analysis. Thermogravimetric/differential thermogravimetric (TG/DTG) analysis of the ILs was performed with a thermogravimetric analyzer, model STD 650 (TA Instruments). Typically, for each analysis about 5 mg of sample was placed in a Pt crucible, and heated from 30 to 600 °C at a constant rate of 10 °C min^{-1} using air as a reactive gas at a flow of 50 mL min^{-1}.

Differential scanning calorimetry. Differential scanning calorimetry (DSC) measurements were performed in a DSC-822e (Mettler Toledo). The DSC curves were performed under dynamic nitrogen atmosphere (50 mL min^{-1}) using 1–6 mg of sample. The runs were performed by heating the samples from 25 up to 120 °C with an isothermal for 20 min, then cooling down until −10 °C at 10 °C min^{-1} with an isothermal of 2 min. Finally heating up to 20 °C at 10 °C min^{-1}.

2.3. Antibacterial activity tests

Cell Culture Conditions and Strains. The strains used for antimicrobial studies were *Staphylococcus aureus* (ATCC 25923), *Escherichia coli* (ATCC 25922), and *Pseudomonas aeruginosa* (ATCC 27853). To do metabolic activation, the frozen bacteria (in skim milk at 20%) were seeded in BHI agar and incubated for 18 h at 37 °C.

Antibacterial Screening. The antibacterial screening was performed with the agar well diffusion (the modified Kirby-Bauer) test [16]. Briefly, plates with 100 mm diameter were prepared using Mueller-Hinton agar (4 mm thick). Once the plates were solidified, a lawn planting was performed from an inoculum of the bacteria (0.5 McFarland). Then, a dry Sensi-Disc (6 mm diameter, Becton Dickinson) previously submerged in a standard (1000 μM) of each compound was placed on the surface. After inverting them, the plates were incubated at 37 °C for 18 h. The inhibition halos, including the diameter of the discs, were subsequently measured. Reference antibiotics were added as a positive control in the form of Sensi-Disc to demonstrate the strain sensitivity, and sterile water was added as a negative control.

Determination of Minimum Inhibitory Concentration (MIC) by Microdilution in 96-Well Plates. The antibacterial activities of the ILs was evaluated by determining their MIC value using 96-well plates and a technique described by Eloff *et al* [17], following the CLSI methods with minor modifications [18]. The bacterial inoculum was obtained from a BHI broth and then adjusted to a final concentration of 10^4–10^5 CFU/mL in Mueller-Hinton broth. The ILs were solubilized in saline (NaCl 0.154 M), and seriated dilutions were made with final concentrations in the range of 1000 μM to 7.81 μM. In each well, 10 μL of the bacterial suspension was aggregated, including positive (bacterial growth) and negative (culture medium) controls.

The different bacteria strains were incubated for 18 h at 37 °C under a continuum stirring, and the bacterial growth was evidenced by adding 2,3,5-triphenyl tetrazolium chloride in each well.

2.4. Molecular simulation

Prediction of the Antimicrobial Properties of ILs. The physicochemical descriptors, ADME (absorption, distribution, metabolism, and excretion), pharmacokinetic properties, drug-like nature, and biocompatibility of the ILs were studied using the SwissADME server [19]. Briefly, 42 descriptors were predicted for each IL, including physicochemical properties, lipophilicity, water solubility, and pharmacokinetics. Based on the descriptors obtained, the acceptability of the compounds based on bioavailability score (drug-likeness) could be assessed [19].

Molecular Dynamics Simulations (MDs). MDs were applied to analyze the interactions between the ILs and membrane bilayers using the Desmond MDs-package,[20] the OPLS3 force field [21], and visual molecular dynamics (VMD) [22]. To perform the two initial MDs, compounds

7a and **8c** were selected because these two ILs presented the lowest and highest MICs against the bacteria we have tested them against, respectively. Both ILs were optimized with OPLS3 force field, and each one was integrated into a single system constructed on an orthorhombic water box (~21,000 TIP3T water model) with dimensions of 88 × 88 × 170 Å^3. The membrane was composed of 70 POPC lipids per layer, and it was placed at 20 Å from the center of mass of the IL. Both systems were maintained at a constant temperature of 323 K and a constant pressure of 1.01325 bar using the NPT ensemble. The SHAKE algorithm [23] was employed for every hydrogen atom, and the cut-off for van der Waals forces was set at 9 Å. The long-range electrostatic forces were modeled using the particle mesh Ewald method. Systems were minimized and equilibrated with the Desmond membrane relaxation protocol and then subjected to 150 ns without any restriction. Data were collected every 2 fs during the MDs.

Next, the interactions between multiple ILs and a POPC membrane model were studied. The ILs selected for the studies were **8c**-ILs because these had better antibacterial activity. A system comprising 52 **8c**-ILs, 122,219 TIP3P water molecules on an orthorhombic water box with dimensions (206 × 147 × 193) Å^3, and a membrane integrated by 364 POPC lipids per layer was constructed. The 52 ILs were positioned at ~ 40 Å from the center of mass of the membrane. The water molecules were selected to be located between 67 Å and 73 Å from the center of mass of the membrane, and a restriction was randomly applied to the majority of the oxygen atoms of water molecules (spring constant = 20 kcal mol^{-1} Å^{-2}). With this "water wall" flowing throughout the system, the ILs were kept to interact only with the upper layer of the membrane. The system was minimized and equilibrated with the Desmond membrane relaxation protocol and then subjected to 2 μs of MDs. The simulation was performed using the same parameters that were used in the 150 ns-MDs.

3. Results

3.1. Synthesis of ILs

A series of ILs containing imidazolium cation and functionalized with phenolic groups are synthesized as illustrated in Scheme 1. The reaction involves a total of three steps and produces a series of *N*-methyl-phenolimidazolium ILs with phenolic groups, which are denoted as **6a-c** – **8a-c**. The reaction steps include hemiaminal formation, aminomethylation and quaternization. The reaction gives the ILs **6a-c** – **8a-c** in 60–87% yield.

The products are then characterized, especially with NMR spectroscopy, mass spectrometry and TG/DTG analysis. As an example, the ^{1}H NMR spectra of **6a** (Fig. 1) shows 11 total signals. The chemical shifts δ 4.64* (s, 2H) and 4.22–4.30** (m, 2H) ppm correspond to methylene groups (–CH$_2$-) that are present in *N*-methylimidazolphenol core and alkyl chain (linker signal: quaternization). The chemical shift δ 1.89–1.91 (m, 2H), 1.34 (s, 6H), and 0.88–0.91 (m, 3H) ppm correspond to the alkyl chain. With the last chemical shifts, the presence of the chain of six carbon atoms stemming from the quaternization reaction between *N*-methylimidazolphenol and bromohexane is confirmed. Additionally, the chemical shifts δ 9.13 (s, 1H), 9.02 (s, 1H), and 8.94 (s, 1H) correspond to the three protons present in the imidazole ring (H2, H4 and H5). Finally, the chemical shifts observed at δ 7.58 (**b**) (d, *J* = 7.6 Hz, 1H), 6.87 (**a**) (t, *J* = 8.7 Hz, 1H), and 6.71–6.74 (**c**) (m, 1H) correspond to compounds containing fluorine.[24] With these results collectively, the formation of the IL **6a** was confirmed.

The thermal stability/properties of the ILs synthesized (**6a-c** to **8a-c**) are studied TG/DTG traces. In their TG/DTG curves, shown in Fig. 2, no major difference, in terms of the maximum decomposition temperature (T_m/°C), is observed for the ILs (see Fig. 2). Their TG/DTG curves also show that their T_m/°C values are in the range 300.51 °C (**8a**) – 318.38 °C (**7c**).

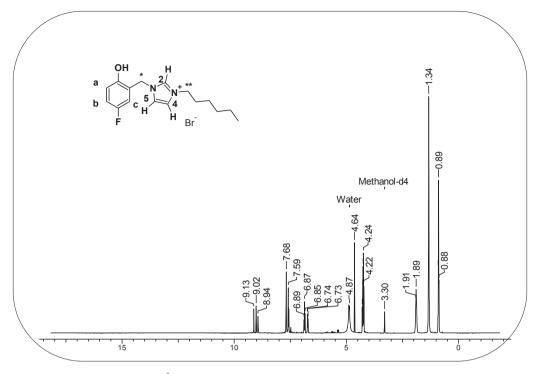The amount of water in the ILs in percentage is calculated based on

Fig. 1. ^{1}H NMR spectrum (400 MHz, CD3OD) of compound **6a**.
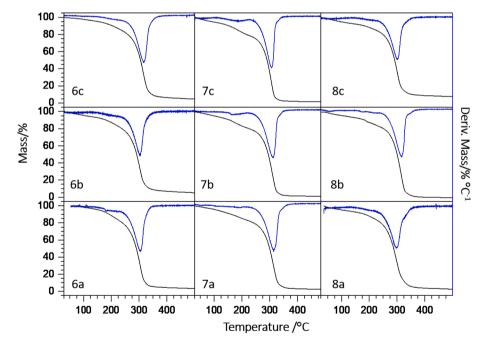

Fig. 2. TG and DTG curves of ILs synthesized and studied.

the weight loss in the region of 50–100 °C in their TG/DTG curves. This corresponds to the water molecules that are physically or weakly bound to the ILs (Fig. 2) [25]. While there are no significant differences in the percentages of water in the ILs possessing different lengths of alkyl chains, interestingly those containing fluorine (**6a-c**) have relatively more adsorbed water than the ILs containing other functional groups (Fig. 3). These physicochemical properties of ILs are attributed to a set of features such as adsorption and miscibility with water [26]. The physicochemical properties of the counterion and cations, and the interactions between them, can also influence their hydrophobicity [27] and their miscibility with water [28].

Additionally, in the DSC curves of the different ionic liquids (**6a-c** to **8a-c**) it is observed melting points (T_m/°C) range of −7.91 to −8.07, −8.24 to −8.40 and −8.39 to −8.40 for the ionic liquids **6a-c**, **7a-c** and **8a-c** series, respectively. These results confirm that the different *N*-methylphenolimidazolium ILs reported here are liquid at room temperature (see support information S49-S57).

3.2. Antibacterial activity

The antimicrobial properties of the series of *N*-alkylimidazolium ILs with phenolic groups synthesized above, **6a-c** – **8a-c**, are then
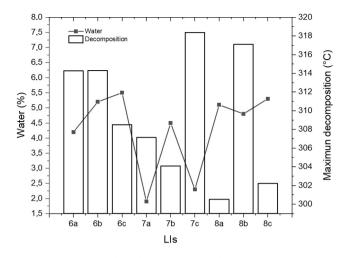
Fig. 3. Comparison of the values of $T_m/°C$ and water contents (%) of the different ILs.

determined. The first screening test is carried out using Sensi-Discs[TM] loaded with each compound at a concentration of 1 μM. The halos of inhibition show that all ILs show antibacterial activity at the concentration they are tested against all bacteria (Table 1). Among them, ILs **6b** and **8a-c** exhibit the maximum inhibition halos against the Gram-positive bacteria *S. aureus*, and their activity is only surpassed by the commercial antibiotic levofloxacin and ceftriaxone. Meanwhile, ILs **8b** and **6a** show the most potent activity against the Gram-negative bacteria *E. coli* and **8a** and **6a** showed the highest activity against *P. aeruginosa*. Their respective antibacterial activities are only surpassed by levofloxacin and ceftriaxone (in case of *E. coli*), and by meropenem, ciprofloxacin, and ceftazidime (in the case of *P. aeruginosa*).

As the concentration used in the initial screening is 1 μM, the MIC values of all ILs are also determined starting with this concentration and using colorimetric assays. The data are reported as the last dilution where the pathogens generate metabolic activity. These studies are done for the bacteria *S. aureus*, *E. coli*, and *P. aeruginosa*, which are responsible

Table 1
Inhibition halos (mm) of different bacteria exposed to the different ILs synthesized and several commercially available antibiotics, which are also tested for comparison.

IL /antibiotics	Inhibition halos (mm)		
	Gram-negative bacteria		Gram-positive bacteria
	E. coli (ATCC 25922)	*P. aeruginosa* (ATCC 27853)	*S. aureus* (ATCC 25923)
6a	34	22	37
6b	31	18	40
6c	28	14	35
7a	28	16	36
7b	29	16	36
7c	29	15	35
8a	29	22	39
8b	35	20	39
8c	33	20	40
Amikacin	21	20	26
Cefotaxime	29	20	30
Ceftazidime	26	23	20
Ceftriaxone	35	19	28
Cefuroxime	23	R[a]	34
Ciprofloxacin	36	25	28
Ertapenem	32	R[a]	26
Gentamicin	25	19	27
Levofloxacin	37	19	28
Meropenem	30	28	34

[a] R represents intrinsic resistance.

for the majority of the nosocomial infections (Table 2). The results show that the IL **8c** present the best MIC values against the Gram-positive bacteria *S. aureus*. Meanwhile, the ILs **8b** and **8c** exhibits the best activity against the Gram-negative bacteria *E. coli* (with a MIC value of 7.81 μM) and the IL **8c** against *P. aeruginosa* (with a MIC value of 125 μM).

3.3. Molecular modeling studies of the ADME properties of ILs and their interactions with cell membranes

The physicochemical descriptors of all ILs are calculated (Table 3). It is worth noting here that all ILs have a MW < 500 g/mol, which is required of compounds to be potentially useful as drugs. All the calculated physicochemical descriptors and pharmacokinetics properties are in the defined acceptable ranges, meeting the criteria of drug-likeness according to Lipinski's rule of five. The calculated properties to predict drug-likeness according to Ghose, Veber, Egan, and Muegge rules [19] (Table 4) show that compounds **6a**, **6b**, **7a**, and **8a** meet the rules but compound **8c** violates four rules.

MDs of the ILs in a POPC bilayer are performed to study their interactions between the ILs and the lipid phase (of microbes). For the first stage of these studies, ILs **7a** and **8c** are selected due to their lower and higher MICs in our antibacterial screening tests, respectively (Table 2). Ligands were immersed in bulk water close to the membrane bilayer and then 150 ns of unrestrained MDs were performed for both ILs. IL **8c** is incorporated onto the bilayer within the first 30 ns and continues interacting with the upper layer for the rest of the simulation. On the other hand, as expected, IL **7a** remains in the water bulk most of the time and then interacts with the upper layer of the membrane at the end of the simulation (~140 ns) (Fig. 4). Meanwhile, IL **8c** interacts faster and for more time with the lipids of the upper layer of the membrane due to its high lipophilicity and topological polar surface area (TPSA). This must be due to the low water solubility of **8c** (Table 3). Therefore, IL **8c** generates a constant interaction with the bilayer during the course of simulations compared with IL **7a**, which has greater solubility in water. A partial density profile of both **7a** and **8c** along the 150 ns simulation time is provided in Fig. 5. The result shows how both ILs reside within a POPC bilayer (represented as POPC phosphates and terminal methyl groups). In both simulations, the quaternary ammonium is found to interact with the phosphate groups of the phospholipids, while the aliphatic moieties extend toward the center of the bilayer. Compound **8c** presents a higher partial density than **7a**, which is consistent with the longer interaction time of **8c** with the upper layer of the membrane.

In 2016, Yoo *et al.* applied coarse-grained MDs to describe how positively charged ILs would affect the morphologies of lipid bilayers [10]. They showed that the asymmetric insertion of IL cations into the upper layer would enhance "leaflet strain", which upon reaching a critical value would trigger disruption in morphologies of the bilayers. In our study, in the second stage of MDs, which we applied to investigate

Table 2
Minimum inhibitory concentration (MIC) of the different ILs synthesized toward different bacteria.

ILs	MIC (μM)		
	Gram-negative bacteria		Gram-positive bacteria
	E. coli (ATCC 25922)	*P. aeruginosa* (ATCC 27853)	*S. aureus* (ATCC 25923)
6a	500	1000	500
6b	15.63	250	62.50
6c	62.50	500	125
7a	500	>1000	500
7b	15.63	500	62.5
7c	15.63	500	15.63
8a	500	1000	250
8b	<7.81	500	31.3
8c	<7.81	125	<7.81

Table 3
Physicochemical and pharmacokinetic descriptors calculated with SwissADME.

ILs	Physicochemical Properties					Lipophilicity	Water Solubility	Pharmacokinetics		
	MW [1]	Rot. Bond [2]	HB-A [3]	HB-D [4]	TPSA [5]	Consensus Log $P_{o/w}$ [6]	Solubility (mol/L)	GI abs [7]	BBB [8]	log K_p (cm/s) [9]
6a	277.36	7	2	1	29.04	2.67	2.38E-05	High	Yes	−5.33
6b	305.41	9	2	1	29.04	3.37	3.79E-06	High	Yes	−4.73
6c	333.46	11	2	1	29.04	4.11	6.10E-07	High	Yes	−4.13
7a	293.81	7	1	1	29.04	2.91	1.11E-05	High	Yes	−5.05
7b	321.86	9	1	1	29.04	3.60	1.78E-06	High	Yes	−4.46
7c	349.92	11	1	1	29.04	4.33	2.87E-07	High	Yes	−3.85
8a	345.5	9	2	1	38.27	3.49	2.25E-06	High	Yes	−4.65
8b	373.55	11	2	1	38.27	4.36	3.66E-07	High	Yes	−4.05
8c	401.61	13	2	1	38.27	5.11	5.97E-08	High	No	−3.45

[1] Molecular weight (g/mol); [2] Number of rotatable bonds; [3] Number of hydrogen bond acceptors; [4] Number of hydrogen bond donors; [5] Topological polar surface area [29]; [6] Average of iLOGP, XLOGP, WLOGP, MLOGP, and SILICOS-IT predictions [19]; [7] Gastrointestinal absorption; [8] Blood-brain barrier permeation; [9] Skin permeation: QSPR model [30].

Table 4
Drug-likeness properties of the ILs as calculated with SwissADME.

ILs	Lipinski # violations [1]	Ghose # violations [2]	Veber # violations [3]	Egan # violations [4]	Muegge # violations [5]
6a	0	0	0	0	0
6b	0	0	0	0	0
6c	0	0	1	0	1
7a	0	0	0	0	0
7b	0	0	0	0	1
7c	0	0	1	0	1
8a	0	0	0	0	1
8b	0	0	1	0	1
8c	0	1	1	1	1

[1] Lipinski (Pfizer) filter [31]: MW ≤ 500; MLOGP ≤ 4.15; N or O ≤ 10; NH or OH ≤ 5. [2] Ghose filter [32]: 160 ≤ MW ≤ 480; −0.4 ≤ WLOGP ≤ 5.6; 40 ≤ MR ≤ 130; 20 ≤ atoms ≤ 70. [3] Veber (GSK) filter [33]: Rotatable bonds ≤ 10; TPSA ≤ 140. [4] Egan (Pharmacia) filter [34]: WLOGP ≤ 5.88; TPSA ≤ 131.6. [5] Muegge (Bayer) filter [35]: 200 ≤ MW ≤ 600; −2 ≤ XLOGP ≤ 5; TPSA ≤ 150; Number of rings ≤ 7; Number of carbon atoms > 4; Number of heteroatoms > 1; Number of rotatable bonds ≤ 15.
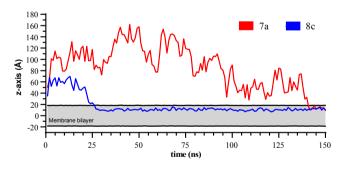

Fig. 4. Distances between ILs **7a** (red), **8c** (blue), and membrane bilayer center of masses as a function of the simulation time. The horizontal black traces correspond to the positions of the lipid bilayer phosphate groups. (For interpretation of the references to colour in this figure legend, the reader is referred to the web version of this article.)

how the active cation of IL **8c** would interact with the membrane, the interaction of fifty-two cations with a POPC membrane bilayer for 2 μs is simulated. Note that compound **8c** is relatively lipophilic as evidenced by an octanol–water partition coefficient of 5.11; however, due to the positively charged quaternary ammonium group in it, the cation is not able to diffuse through the membrane. Our results show that one insertion mechanism is preferred. First, among the ILs clustered forming aggregates (small micelles), three clusters are identified in our 2 μs MDs, namely clusters 1 and 2, which are composed of thirteen molecules each, and cluster 3, which is composes of twenty ILs. The remaining six ILs insert spontaneously and independently along the simulation (Figs. 6

and 7). The micelle formation occurs within the first 30 ns of the simulation (Fig. 7), and then cluster 1 starts to interact with the membrane upper layer after 56 ns (Figs. 6 and 7) and spontaneous insertions happens at ∼ 67 ns (Fig. 8). Cluster 2 starts to interact with the membrane after the first 100 ns and then the insertion takes place (Figs. 6 and 8). Finally, while cluster 3 remains in the water bulk section most of the time, it interacts with the upper bilayer and after ∼ 1.7 μs cluster insertion ensues (Figs. 6 and 7). In all cluster insertion events, and also when the **8c**-IL molecules are inserted individually, the ILs molecules are disaggregated (laterally) after insertion within the upper layer of the membrane (Fig. 7).

4. Discussion

In this work, a series of *N*-methylphenolimidazolium ILs **6a-c** – **8a-c** are obtained, and their antimicrobial properties are studied. Their reactivity and yields after synthesis are also included. For better understanding of the synthetic plan, the synthesis of the IL 1-(5-fluoro-2-hydroxybenzyl)-3-hexyl-1*H*-imidazol-3-ium bromide (**6a**) is described in detail, as an example (Scheme 1). The synthesis begins with the formation of hemiaminal **2**, which is obtained from the reaction between imidazole **1** and paraformaldehyde in a 5:5 mmol ratio and 3 mL of THF. The reaction mixture is stirred and then subjected to MW (200 W) at 120 °C for 5 min. It gives a colorless oily product, IL **3**, in 80% yield as determined based on GC–MS analysis.

Then, following the observations of DeBerardinis *et al.* [36], with slight modifications, the

aminomethylation reaction between hemiaminal **3** and 4-fluorophenol **4a**, in a 5:5 mmol ratio, is directly conducted under microwave condition. As a solvent, dioxane/H_2O in a 1:1 ratio (1 mL) is used. This condensation reaction occurs without the presence of catalysts.

It should be noted that this type of condensation was reported by DeBerardinis *et al.* [36] at reflux with a reaction time of 17 h, while our variant, proceeds in microwaves in only 5 min of reaction. After the reaction is completed, the product is extracted using DCM, dried with Na_2SO_4, concentrated under reduced pressure, and purified by column chromatography (hexane/AcOEt 7:3) to afford the *N*-methylphenolimidazole **5a** (90% yield). Finally, **5a** (1 mmol) is mixed with bromohexane (1.5 mmol) under solvent-free condition and microwaved at 200 MW at 80 °C for 5 min, as was described in previous work [14,37]. Reaction completion is marked when a dense IL is separated, which is subsequently isolated using toluene and by decantation. Any unreacted starting materials and solvents are also removed along with toluene. Subsequently, the IL is rinsed with diethyl ether (4 × 3 mL) separating the bottom layer afterward by decantation and subsequently subjected to high vacuum for 4 h to afford the IL **6a** (73% yield). The structure of **6a** is confirmed on basis of ^{1}H NMR analysis.

The thermal stability test results show that all of the ILs have low thermal stability and almost similar degradation temperature profiles. In
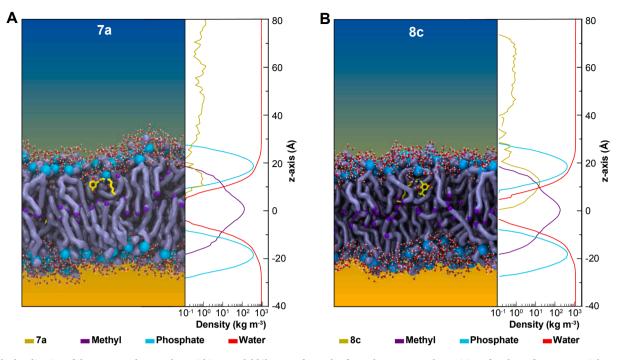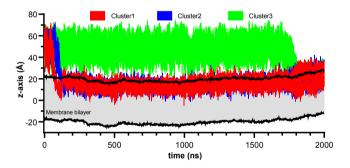
Fig. 5. The localization of the compounds **7a** and **8c** within a model bilayer. Left panels of A and B represent the position of each IL after 150 ns. Right panels of A and B represents the partial density profiles for both ILs (yellow), as well as the water bulk (red lines) and membrane bilayer phosphate groups (cyan) and terminal methyl groups (purple). (For interpretation of the references to colour in this figure legend, the reader is referred to the web version of this article.)

Fig. 6. Distances between **8c** IL and the center of mass of a membrane bilayer as a function of the simulation time. The black traces correspond to the positions of the lipid phosphates in both layers.

other words, there show no significant difference in the decomposition temperature profiles even if their alkyl chain length changes. This can be explained on the basis of the hygroscopic properties and miscibility in water of their imidazolium cations, which have the ability to adsorb water at room temperature [38]. This hydration is explained by the interactions involving imidazolium ring, mainly with the H2, H4 and H5 atoms (see Fig. 1), and water molecules [39], which contributes to the maximum decomposition temperature of water present in the ILs [26].

The efficacy of the ILs against different bacterial is then investigated. Not surprisingly, the ILs generally affected the Gram-positive bacteria more than the Gram-negative ones. The Gram-negative bacteria (*P. aeruginosa* and *E. coli*) are generally more resistant to the ILs because they are composed of two membranes: a thin membrane of peptidoglycan and an outer membrane [40]. For its part, the cell membrane of (Gram-positive) bacterium (*S. aureus*) is comprised of peptidoglycan and teichoic acid, an essential polyanionic polymer of the cell wall that is responsible for the structural stability of this bacteria [41]. Our results
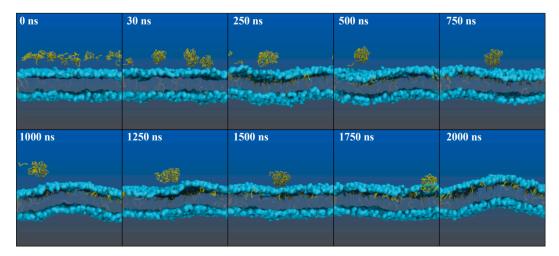

Fig. 7. Overview of molecular dynamics simulation (MD) of the molecules of compound **8c** within a model bilayer for 2 μs.
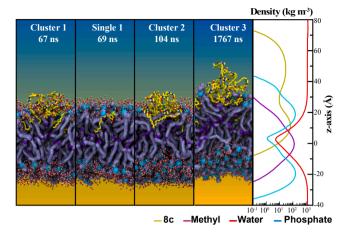
Fig. 8. The localization of the **8c**-ILs (fifty-two molecules) within a model bilayer along the 2 μs-MDs. The key interactions for all clusters and single molecules are shown at a specific time. The right panel represents the partial density profile for all ILs as well as the water bulk (red curve) membrane bilayer POPC phosphate groups (cyan curve), and terminal methyl groups (purple curve). (For interpretation of the references to colour in this figure legend, the reader is referred to the web version of this article.)

are in concordance with one reported by Elshaarawy and Janiak [42], which showed that metallosaldache-imidazolium salts exhibited a better antimicrobial activity against Gram-positive bacteria. And, they attributed this to the structural differences between the cell-walls of Gram-positive bacteria and the Gram-negative bacteria.

The antibacterial activity of the ILs is also found to be dependent on the length of their alkyl chains (**a** to **c**). Łuczak *et al.* studied the effects of the chain length and anion type of ILs of different imidazolium ILs on their antibacterial activity.[43] They found that the introduction of a longer chain in the imidazolium cation gives a lower MIC value, with a cut-off at a chain length of sixteen or eighteen carbons for the imidazolium cation and Cl⁻ anion. In another work, Gundolf *et al.* studied the influence of the lipopolysaccharides (LPS) of the Gram-negative bacteria on the efficacy of antimicrobial ILs, by specifically considering the chain length in the ILs as a variable [44]. Specifically, they explored the modifications in the length of LPS and its effect on the susceptibility of *E. coli* K-12 due to the ILs and three different single-gene deletion mutants. To do so, the authors tested imidazolium ([$C_n$mim]Cl) and ammonium-based ([TMC$_n$A]Cl) ILs with varying alkyl side chain lengths (C_{10} – C_{16}) as representatives of ILs with one alkyl side chain. Their results indicated that length of LPS would strongly affect the degree of resistance of the microbe towards ILs with one alkyl side chain. The most effective ILs were found to be those with a chain length of sixteen carbons (namely, [C_{16}mim]Cl and [TMC$_{16}$A]Cl).

In our case, the incorporation of Cl or F groups in the phenolic ring of IL is not found to exert a considerable effect on the antibacterial activity of the ILs (**6a-c** versus **7a-c**). Moreover, in case of **6c**, was observed a reduction in the antibacterial activity. In this particular case a positive tendency among the MIC value and the increased in the chain length was observed until eight carbons (**6b**) to then decrease. Comparing the different series synthesized, show us that probably the use of an halogen in the phenolic ring is not a good choice (serie **6** and **7**) due to in case of the serie **7** where Cl⁻ was chosen, the MIC value only follow a tendency until a chain length of eight carbons (**7b**), to then maintain the antibacterial activity with a chain length of ten carbons (in Gram-negative bacteria), meanwhile, when the halogen was changed by F⁻ the antibacterial activity decrease with an alkyl length of ten carbons, probably due to the influence of the halogen in the phenolic ring; this was demonstrated when the halogen in the phenolic ring was changed by OCH$_3$ (serie **8**), in this case the antibacterial activity not only showed a tendency with the increased of the alkyl chain, but also showed an

increment in the potency of the compound among all the studied bacteria. In any case, more studies are necessary to clarify the effect that the halogen of the phenolic ring may have on the structure of the synthesized ILs and its influence on the antibacterial activity.

Meanwhile, the incorporation of a more lipophilic substituent as OCH$_3$ and a second alkyl chain (C(CH$_3$)$_3$) in the phenolic ring (**8a-c**) is found to enhance the antibacterial activity, giving MIC values of < 7.81 μM for the Gram-positive bacteria and 125 μM for the Gram-negative bacteria (**8c**). It has been reported that the hydrophobic anions and longer alkyl chains provide more potent biological activities in ILs [45] and other compounds [46]. This may be why the incorporation of OCH$_3$ and a second alkyl chain in ILs render improved antibacterial activity to the synthesized ILs.

Physicochemical descriptors are calculated for all ILs studied in this work, including MW, the total number of hydrogen bond acceptors (HB-A) and donors (HB-D), and the TPSA. In addition, lipophilicity, water solubility, and pharmacokinetics properties of all ILs are determined. Based on the results, compound **8c** is found to violate four rules in total because of the high number of its rotatable bonds due to its long aliphatic chain ($n = 7$), methoxy group (–OCH$_3$) and *tert*-butyl radical (-C(CH$_3$)). The rotatable bonds of **8c** are within the limit, though; therefore, **8c** as well as the other ILs evaluated here, are considered to have acceptable properties that are likely to make them suitable for as oral drugs for human use.

The density distributions of all (fifty-two) ILs of **8c** along the bilayer normal can be compared with the location of the lipid headgroups and tails (Fig. 8). These density profiles show that all inserted ILs do not diffuse through the membrane. Moreover, half of the population remains in the aqueous phase during most of the simulation time while the other half interacts with the membrane and remains at the bottom of the limit established by the POPC phosphate groups. The results indicate that the insertion of ILs occurs mostly by small clusters, followed by lateral disintegration, possibly until the membrane is saturated with them. Based on other studies [10] in the next process, the IL membrane saturation leads to an increase in the tension in the upper bilayer up to the critical threshold, possibly prompting the morphological disruption of the membrane. So, to demonstrate how the morphology of the membrane is affected by **8c**, longer simulations must be performed using other methods such as coarse-grained molecular dynamics simulations. This may allow the simulation of systems with >1000 ILs and for a longer time (up to 10^2 μs). The result may provide additional insights into the mechanisms involved in the antibacterial effects of ILs and thereby enabling further design of efficacious antimicrobial agents in the future.

5. Conclusions

Nosocomial infections are among the major health threats the public currently faces worldwide. Therefore, there is a great need to develop new antimicrobial agents that can tackle this issue. To this end, in this work, we have synthesized and studied the antibacterial properties of a series of ILs containing *N*-alkylimidazolium cations with phenolic functional groups and different substituents. The ILs were synthesized using microwave-assisted approach. The synthesis involved three reaction steps, including hemiaminal formation, followed by aminomethylation, and finally alkyl quaternization reaction, all of which employing microwaves. The resulting ILs showed antibacterial activity against *S. aureus*, *E. coli*, and *P. aeruginosa*, which are responsible for the majority of the nosocomial infections. The MIC values ranged from < 7.81 to 62.50 μM, being better for **8b** and **8c** (<7.81 μM). The alkyl chain length and substituents on the phenolic ring were found to affect the antibacterial efficacies of the ILs. Molecular dynamics simulations of ILs in a POPC bilayer were performed to study the interactions between the ILs and the lipid phase of the microbes' membranes. The results showed key features in the mechanism of IL-induced membrane disruption. Notably, the ILs were found to insert clusters into one side of the bilayer until saturation was reached. This insertion then increased

"leaflet strain" up to critical threshold, possibly triggering the morphological disruption of the membranes in the microbes.

Declaration of Competing Interest

The authors declare that they have no known competing financial interests or personal relationships that could have appeared to influence the work reported in this paper.

Acknowledgement

Appendix A. Supplementary material

Supplementary data to this article can be found online at https://doi.org/10.1016/j.bioorg.2021.105289.

References

[1] S.Y. Tong, J.S. Davis, E. Eichenberger, T.L. Holland, V.G. Fowler, Staphylococcus aureus infections: epidemiology, pathophysiology, clinical manifestations, and management, Clin. Microbiol. Rev. 28 (3) (2015) 603–661.

[2] D.R. Jenkins, Nosocomial infections and infection control, Medicine 45 (10) (2017) 629–633.

[3] T. Welton, Ionic liquids: a brief history, Biophys. Rev. 10 (3) (2018) 691–706.

[4] K.S. Egorova, E.G. Gordeev, V.P. Ananikov, Biological Activity of Ionic Liquids and Their Application in Pharmaceutics and Medicine, Chem Rev 117 (10) (2017) 7132–7189.

[5] E. Guibal, T. Vincent, C. Jouannin, Immobilization of extractants in biopolymer capsules for the synthesis of new resins: a focus on the encapsulation of tetraalkyl phosphonium ionic liquids, J. Mater. Chem. 19 (45) (2009) 8515–8527.

[6] K.A. Kurnia, T.E. Sintra, C.M.S.S. Neves, K. Shimizu, J.N. Canongia Lopes, F. Gonçalves, S.P.M. Ventura, M.G. Freire, L.M.N.B.F. Santos, J.A.P. Coutinho, The effect of the cation alkyl chain branching on mutual solubilities with water and toxicities, Phys. Chem. Chem. Phys. 16 (37) (2014) 19952–19963.

[7] Y. Wang, H. Li, S. Han, A Theoretical Investigation of the Interactions between Water Molecules and Ionic Liquids, J. Phys. Chem. B 110 (48) (2006) 24646–24651.

[8] J. Gravel, A.R. Schmitzer, Transmembrane anion transport mediated by adamantyl-functionalised imidazolium salts, Supramol. Chem. 27 (5–6) (2015) 364–371.

[9] C.R. Elie, G. David, A.R. Schmitzer, Strong Antibacterial Properties of Anion Transporters: A Result of Depolarization and Weakening of the Bacterial Membrane, J. Med. Chem. 58 (5) (2015) 2358–2366.

[10] B. Yoo, Y. Zhu, E.J. Maginn, Molecular mechanism of ionic-liquid-induced membrane disruption: morphological changes to bilayers, multilayers, and vesicles, Langmuir 32 (21) (2016) 5403–5411.

[11] T. Welton, Room-Temperature Ionic Liquids. Solvents for Synthesis and Catalysis, Chem. Rev. 99 (8) (1999) 2071–2084.

[12] S. Aher, P. Bhagat, Convenient synthesis of imidazolium based dicationic ionic liquids, Res. Chem. Intermed. 42 (6) (2016) 5587–5596.

[13] S. Morales-Navarro, L. Prent-Peñaloza, Y.A. Rodríguez Núñez, L. Sánchez-Aros, O. Forero-Doria, W. González, N.E. Campilllo, M. Reyes-Parada, A. Martínez, D. Ramírez, Theoretical and Experimental Approaches Aimed at Drug Design Targeting Neurodegenerative Diseases, Processes 7 (12) (2019) 940.

[14] O. Forero Doria, R. Castro, M. Gutierrez, D. Gonzalez Valenzuela, L. Santos, D. Ramirez, L. Guzman, Novel Alkylimidazolium Ionic Liquids as an Antibacterial Alternative to Pathogens of the Skin and Soft Tissue Infections, Molecules 23 (9) (2018).

[15] K. Murakami, S. Ohnishi, T. Yano, M. Itoh, Azolyl methyl phenyl derivatives having aromatase inhibitory activity, Google Patents (1996).

[16] J.J. Biemer, Antimicrobial susceptibility testing by the Kirby-Bauer disc diffusion method, Ann. Clin. Lab. Sci. 3 (2) (1973) 135–140.

[17] J.N. Eloff, A sensitive and quick microplate method to determine the minimal inhibitory concentration of plant extracts for bacteria, Planta Med. 64 (08) (1998) 711–713.

[18] P. Wayne, Clinical and Laboratory Standarts Institute: methods for dilution antimicrobial susceptibility tests for bacteria that grow aerobically, Approved Standart M7-A7, CLSI, USA, 2006.

[19] A. Daina, O. Michielin, V. Zoete, SwissADME: a free web tool to evaluate pharmacokinetics, drug-likeness and medicinal chemistry friendliness of small molecules, Sci. Rep. 7 (2017) 42717.

[20] K.J. Bowers, D.E. Chow, H. Xu, R.O. Dror, M.P. Eastwood, B.A. Gregersen, J.L. Klepeis, I. Kolossvary, M.A. Moraes, F.D. Sacerdoti, Scalable algorithms for molecular dynamics simulations on commodity clusters, SC'06: Proceedings of the 2006 ACM/IEEE Conference on Supercomputing, IEEE, 2006, pp. 43-43.

[21] E. Harder, W. Damm, J. Maple, C. Wu, M. Reboul, J.Y. Xiang, L. Wang, D. Lupyan, M.K. Dahlgren, J.L. Knight, OPLS3: a force field providing broad coverage of drug-like small molecules and proteins, J. Chem. Theory Comput. 12 (1) (2015) 281–296.

[22] W. Humphrey, A. Dalke, K. Schulten, VMD: visual molecular dynamics, J. Mol. Graph. 14 (1) (1996) 33–38.

[23] V. Kräutler, W.F. Van Gunsteren, P.H. Hünenberger, A fast SHAKE algorithm to solve distance constraint equations for small molecules in molecular dynamics simulations, J. Comput. Chem. 22 (5) (2001) 501–508.

[24] J.-R. Wang, K. Manabe, High Ortho Preference in Ni-Catalyzed Cross-Coupling of Halophenols with Alkyl Grignard Reagents, Org. Lett. 11 (3) (2009) 741–744.

[25] F. Avila-Salas, Y.A. Rodríguez Nuñez, A. Marican, R.I. Castro, J. Villaseñor, L.S. Santos, S. Wehinger, E.F. Durán-Lara, Rational development of a novel hydrogel as a pH-sensitive controlled release system for nifedipine, Polymers 10 (7) (2018) 806.

[26] J.G. Huddleston, A.E. Visser, W.M. Reichert, H.D. Willauer, G.A. Broker, R.D. Rogers, Characterization and comparison of hydrophilic and hydrophobic room temperature ionic liquids incorporating the imidazolium cation, Green Chem. 3 (4) (2001) 156–164.

[27] A.E. Visser, R.P. Swatloski, W.M. Reichert, S.T. Griffin, R.D. Rogers, Traditional extractants in nontraditional solvents: Groups 1 and 2 extraction by crown ethers in room-temperature ionic liquids, Ind. Eng. Chem. Res. 39 (10) (2000) 3596–3604.

[28] C. Hanke, R. Lynden-Bell, A simulation study of water− dialkylimidazolium ionic liquid mixtures, J. Phys. Chem. B 107 (39) (2003) 10873–10878.

[29] P. Ertl, B. Rohde, P. Selzer, Fast calculation of molecular polar surface area as a sum of fragment-based contributions and its application to the prediction of drug transport properties, J. Med. Chem. 43 (20) (2000) 3714–3717.

[30] R.O. Potts, R.H. Guy, Predicting skin permeability, Pharm. Res. 9 (5) (1992) 663–669.

[31] C.A. Lipinski, F. Lombardo, B.W. Dominy, P.J. Feeney, Experimental and computational approaches to estimate solubility and permeability in drug discovery and development settings, Adv. Drug Deliv. Rev. 23 (1–3) (1997) 3–25.

[32] A.K. Ghose, V.N. Viswanadhan, J.J. Wendoloski, A knowledge-based approach in designing combinatorial or medicinal chemistry libraries for drug discovery. 1. A qualitative and quantitative characterization of known drug databases, J. Comb. Chem. 1 (1) (1999) 55–68.

[33] D.F. Veber, S.R. Johnson, H.-Y. Cheng, B.R. Smith, K.W. Ward, K.D. Kopple, Molecular properties that influence the oral bioavailability of drug candidates, J. Med. Chem. 45 (12) (2002) 2615–2623.

[34] W.J. Egan, K.M. Merz, J.J. Baldwin, Prediction of drug absorption using multivariate statistics, J. Med. Chem. 43 (21) (2000) 3867–3877.

[35] I. Muegge, S.L. Heald, D. Brittelli, Simple selection criteria for drug-like chemical matter, J. Med. Chem. 44 (12) (2001) 1841–1846.

[36] A.M. DeBerardinis, M. Turlington, J. Ko, L. Sole, L. Pu, Facile synthesis of a family of H8BINOL-amine compounds and catalytic asymmetric arylzinc addition to aldehydes, J. Organic Chem. 75 (9) (2010) 2836–2850.

[37] O. Forero Doria, R. Castro, M. Gutierrez, D. Gonzalez Valenzuela, L. Santos, D. Ramirez, L. Guzman, Novel alkylimidazolium ionic liquids as an antibacterial alternative to pathogens of the skin and soft tissue infections, Molecules 23 (9) (2018) 2354.

[38] S. Cuadrado-Prado, M. Dominguez-Perez, E. Rilo, S. Garcia-Garabal, L. Segade, C. Franjo, O. Cabeza, Experimental measurement of the hygroscopic grade on eight imidazolium based ionic liquids, Fluid Phase Equilib. 278 (1–2) (2009) 36–40.

[39] A. Mele, C.D. Tran, S.H. De Paoli Lacerda, The Structure of a Room-Temperature Ionic Liquid with and without Trace Amounts of Water: The Role of C-H⋯ O and C-H⋯ F Interactions in 1-n-Butyl-3-Methylimidazolium Tetrafluoroborate, Angew. Chem. Int. Ed. 42 (36) (2003) 4364–4366.

[40] M. Kong, X.G. Chen, C.S. Liu, C.G. Liu, X.H. Meng, l.J. Yu, Antibacterial mechanism of chitosan microspheres in a solid dispersing system against E. coli, Colloids Surf B Biointerfaces 65(2) (2008) 197-202.

[41] D. Raafat, K. von Bargen, A. Haas, H.G. Sahl, Insights into the mode of action of chitosan as an antibacterial compound, Appl Environ Microbiol 74 (12) (2008) 3764–3773.

[42] R.F. Elshaarawy, C. Janiak, Toward new classes of potent antibiotics: synthesis and antimicrobial activity of novel metallosaldach-imidazolium salts, Eur J Med Chem 75 (2014) 31–42.

[43] J. Łuczak, C. Jungnickel, I. Łącka, S. Stolte, J. Hupka, Antimicrobial and surface activity of 1-alkyl-3-methylimidazolium derivatives, Green Chem. 12 (4) (2010) 593–601.

[44] T. Gundolf, B. Rauch, R. Kalb, P. Rossmanith, P. Mester, Influence of bacterial lipopolysaccharide modifications on the efficacy of antimicrobial ionic liquids, J. Mol. Liq. 271 (2018) 220–227.

[45] O.B. Ghanem, S.N. Shah, J.-M. Lévêque, M.I.A. Mutalib, M. El-Harbawi, A.S. Khan, M.S. Alnarabiji, H.R.H. Al-Absi, Z. Ullah, Study of the antimicrobial activity of cyclic cation-based ionic liquids via experimental and group contribution QSAR model, Chemosphere 195 (2018) 21–28.

[46] J. Echeverría, A. Urzúa, L. Sanhueza, M. Wilkens, Enhanced Antibacterial Activity of Ent-Labdane Derivatives of Salvic Acid (7α-Hydroxy-8(17)-ent-Labden-15-Oic Acid): Effect of Lipophilicity and the Hydrogen Bonding Role in Bacterial Membrane Interaction, Molecules 22 (7) (2017).